PROCEEDINGS OF SCIENCE

A study of the pion and the kaon TMDPDFs in twisted mass lattice QCD

Constantia Alexandrou,[a,b] **Simone Bacchio,**[b] **Krzysztof Cichy,**[c] **Martha Constantiou,**[d] **Xu Feng,**[e] **Kyriakos Hadjiyiannakou,**[a,b] **Karl Jansen,**[f] **Chuan Liu,**[e] **Aniket Sen,**[g] **Gregoris Spanoudes,**[b] **Fernanda Steffens**[g] **and Jacopo Tarello**[a,b,*]

[a] *Department of Physics, University of Cyprus, P.O. Box 20537, 1678 Nicosia, Cyprus*

[b] *Computation-based Science and Technology Research Center, The Cyprus Institute, 20 Kavafi Street, Nicosia 2121, Cyprus*

[c] *Faculty of Physics, Adam Mickiewicz University ul. Uniwersytetu Poznańskiego 2, 61-614 Poznań, Poland*

[d] *Department of Physics, Temple University, Philadelphia, PA 19122 - 1801, USA*

[e] *School of Physics, Peking University (PKU), No.5 Yiheyuan Road, Haidian Distric, Beijing, 100871, China*

[f] *Deutsches Elektronen-Synchrotron (DESY), Platanenallee 6, 15738 Zeuthen, Germany*

[g] *Rheinische Friedrich-Wilhelms-Universität Bonn, Helmholtz-Institut für Strahlen- und Kernphysik,Nußallee 14-16,53115 Bonn, Germany*

E-mail: j.tarello@cyi.ac.cy

We compute the pion and kaon matrix elements that yield the transverse-momentum-dependent parton distribution functions. We use an $N_f = 2 + 1 + 1$ twisted mass fermion ensemble of lattice size 24^3x48, lattice spacing $a = 0.093$ fm, and a pion mass of 350 MeV. We employ momentum smearing to improve the signal of the boosted pion and kaon states. We also study the mixing pattern of the extended operators with an asymmetric Wilson staple under renormalization and implement an RI/MOM scheme for the non-perturbative renormalization.

The 39th International Symposium on Lattice Field Theory, LATTICE2022 8th-13th August, 2022, University of Bonn, Germany

*Speaker

PoS(LATTICE2022)273

1. Introduction

The internal structure of hadrons has been the subject of studies both theoretically and experimentally. One of the quantities that provide information on the 3-dimensional structure of hadrons are the transverse-momentum-dependent parton distribution functions (TMDPDFs) [1].

The computation of these quantities in lattice QCD intensified with the development of the large momentum effective field theory (LaMET) [2] (see Refs. [3–7] for recent reviews). In such a framework, TMDPDFs can be written in terms of a rapidity-dependent part, namely the Collins-Soper kernel, and rapidity-independent parts, comprising the soft function and the quasi-beam function [4, 8]. In this work, we will focus on the calculation of the quasi-beam function of the pion and the kaon.

Specifically, we present results on the pion and kaon matrix elements of non-local quark bilinear operators with staple-shaped Wilson lines. These are renormalized employing an RI/MOM scheme and using symmetry arguments to disentagle the mixing pattern [9].

2. Lattice Setup

2.1 Lattice Characteristics

The ensemble of gauge field configurations used in this work was generated by the Extended Twisted Mass Collaboration (ETMC) [10] using clover-improved twisted mass fermions and the Iwasaki gauge action. The simulated pion mass corresponds to 350 MeV and the kaon mass to 554 MeV. The hadron boost used in this work for both mesons is $a\boldsymbol{p} = \{0, 0, 2\}2\pi/L$ in the arbitrary $\hat{n}_z$ direction, which corresponds in physical units to $|\boldsymbol{p}| \approx 1.11$ GeV. The parameters used for the simulations are given in Table 1.

Ensemble name	$L^3 \times T$	a (fm)	$a\mu_l$	m_π (MeV)	$a\mu_s$	m_K (MeV)
cA211.53.24	$24^3 \times 48$	0.093	0.0053	350	0.0221	554

$a\boldsymbol{p}$	$\|\boldsymbol{p}\|$ (GeV)	t_{sep}/a	N_{confs}	N_{source}
$\{0, 0, 2\}2\pi/L$	1.11	6, 8, 10	300	10

Table 1: Top: Parameters used in the ensemble simulation with the columns being, respectively, i) the ensemble name, ii) the lattice volume, iii) the lattice spacing, iv) the light bare quark mass, v) the pion mass m_π, vi) the strange bare quark mass, and vii) the kaon mass m_K. Bottom: Statistics used in the calculation with the columns being, respectively, i) the lattice hadron boost $\boldsymbol{p}$ used for all our matrix elements results for both pion and kaon, ii) the magnitude of such hadron boost in physical units, iii) the employed source-sink separations, iv) the number of configurations used to calculate the matrix elements, and v) the number of source-positions used for each configuration.

2.2 Correlation functions and matrix elements

The quasi-beam function is defined by the following matrix element,

$$B^{\Gamma}(x, \boldsymbol{p}; b, z, l) = \langle M(\boldsymbol{p})|\bar{\psi}(x)\,\Gamma\mathcal{W}\psi(x + b\hat{n}_\perp + z\hat{n}_z)\,|M(\boldsymbol{p})\rangle, \tag{1}$$

with $M(\boldsymbol{p})$ referring to above being the mesonic state with boost $\boldsymbol{p} = (0, 0, p_z)$, ψ the quark field and $\mathcal{W}$ the staple-shaped Wilson line whose definition is given by

$$\mathcal{W}(b, z, l) = W_z^{\dagger}(\boldsymbol{x} - l\hat{n}_z, l)\, W_{\perp}(\boldsymbol{x} - l\hat{n}_z, b)\, W_z(\boldsymbol{x} - l\hat{n}_z + b\hat{n}_T, (l + z)), \tag{2}$$

with $W_i(\boldsymbol{x}, L)$ being the Wilson line starting from position $\boldsymbol{x}$ and going in the direction $\hat{n}_i$ for a distance L. The longitudinal parts W_z of this asymmetric staple are taken parallel to the direction of the boost of the hadron, whereas the perpendicular one $W_{\perp}$ goes along one of the transverse direction, either $\hat{n}_x$ or $\hat{n}_y$. By argument of rotational invariance, in this preliminary study we selected the transverse direction $\hat{n}_{\perp} = \hat{n}_x$. A graphical representation of $\mathcal{W}(b, z, l)$ is given in the left-hand-side of Fig. 1.

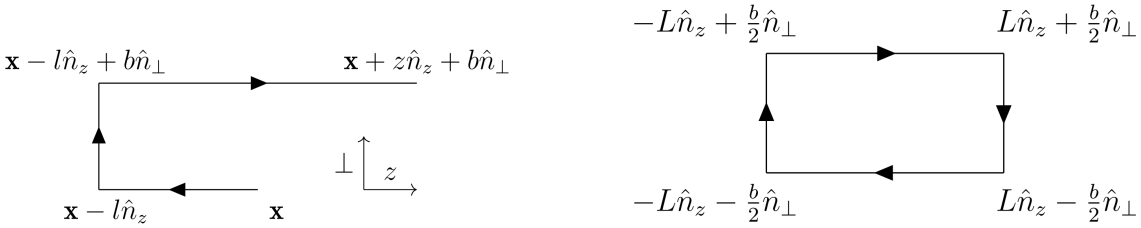

Figure 1: Graphical representation of the asymmetric staple (left) and Wilson loop (right).

In order to extract the lattice matrix elements, we calculate three-point functions with a staple-shaped operator and two-point functions for each meson. We employ momentum-smeared interpolating fields improving the signal-to-noise ratio for boosted meson states [11]. The parameters for the Gaussian smearing [12] are $n_{\text{gauss}} = 50$ and $\alpha_{\text{gauss}} = 4.0$ and for the momentum smearing $\xi = 0.6$, which is tuned in order to provide the best signal-to-noise ratio for both mesons. Also, the gauge links entering the Gaussian smearing are APE-smeared [13] with parameters $n_{\text{APE}} = 50$ and $\alpha_{\text{APE}} = 0.5$. We take $J_{\pi^+}(x) = \bar{d}\gamma_5 u$ for the interpolator field of π^+ and $J_{K^+}(x) = \bar{s}\gamma_5 u$ for K^+.

We construct two- and three-point correlation functions with the non-local bilinear operator with staple-shaped Wilson line which is stout-smeared [14] with parameters $n_{\text{stout}} = 5$ and $\rho_{\text{stout}} = 0.1315$. Since we employ point-sources in our lattice calculations, the correlation functions are given by

$$C_{2pt}^{M}(t, \mathbf{p}) = \sum_{\mathbf{x}} e^{-i\boldsymbol{p}\cdot(\boldsymbol{x}-\boldsymbol{x_0})} \langle J_M(x) J_M^{\dagger}(x_0) \rangle, \tag{3}$$

$$C_{3pt}^{M,\psi}(t, t_s, \mathbf{p}, \Gamma, b, z, l) = \sum_{\mathbf{x},\mathbf{x_f}} e^{-i\boldsymbol{p}\cdot(\boldsymbol{x_f}-\boldsymbol{x_0})} \langle J_M(x_f) \bar{\psi}(x) \Gamma \mathcal{W}(b, z, l) \psi(x + b\hat{n}_{\perp} + z\hat{n}_z) J_M^{\dagger}(x_0) \rangle, \tag{4}$$

where M stands for the particular meson under analysis, x_0 denotes the smeared point-source, t_s is the time separation between the source and the sink, and ψ either the light or strange quark at the insertion operator.

The matrix elements can be extracted by employing the ratio of the three-point to the two-point functions taking into account the periodicity of the two-point function. Namely, the two-point function, assuming ground state dominance, is given by

$$C_{2pt} = c_0 \left(e^{-E_0^{\boldsymbol{p}} t} + e^{-E_0^{\boldsymbol{p}}(T-t)} \right), \tag{5}$$

where T is the temporal lattice extent. Knowing this behaviour for the two-point function, we can then fit our results in order to extract the overlap with the ground state c_0 and the ground state energy $E_0^{\boldsymbol{p}}$ and use them to form the following ratio:

$$\frac{C_{3pt}^{M,\psi}}{c_0 e^{-E_0^{\boldsymbol{p}} t_f}} \overset{t,t_s \to \infty}{\longrightarrow} K(p,\Gamma) h_\Gamma^{M}{}_{\psi}, \tag{6}$$

where C_{3pt}^{M} is the three-point function, h_Γ is the desired matrix element and $K(p,\Gamma)$ is a kinematic factor depending on the hadron momentum and insertion operator Γ. For all the results presented in this work, we consider only the connected contributions for both the pion π^+ and kaon K^+.

The staple-shaped Wilson line introduces linear and logarithmic (cusp and end-point) divergences in the three-point function for non-zero values of both b, l and z parameters [4]. One way to remove the linear and cusp divergences is to divide the three-point function by the square root of the vacuum expectation value of the Wilson loop Z_E given by (for a graphical representation, see Fig. 1) [15]

$$Z_E(b,l) = \frac{1}{N_c}\left\langle W_\perp\left(-l\hat{n}_z - \frac{b}{2}\hat{n}_\perp, b\right) W_z\left(-l\hat{n}_z + \frac{b}{2}\hat{n}_\perp, 2l\right) W_\perp^\dagger\left(l\hat{n}_z - \frac{b}{2}\hat{n}_\perp, b\right) W_z^\dagger\left(-l\hat{n}_z - \frac{b}{2}\hat{n}_\perp, 2l\right)\right\rangle. \tag{7}$$

The remaining end-point divergences can be eliminated by employing, e.g., RI/MOM renormalization scheme (see next section). However, since the vertex functions in the RI/MOM conditions have the same linear and logarithmic divergences, the RI/MOM renormalization functions can cancel all divergences in the bare matrix elements without the use of Z_E.

2.3 Renormalization

The bare quasi-beam function is renormalized non-perturbatively by using the RI/MOM scheme [16]. We define the renormalization functions for the quark field $Z_q^{\mathrm{RI/MOM}}$ and for the staple-shaped operators $Z_{\Gamma\Gamma'}^{\mathrm{RI/MOM}}$ by imposing the following renormalization conditions:

$$Z_q^{\mathrm{RI/MOM}}(\mu_0) = -i\frac{\mathrm{Tr}\left[\sum_\mu S(p)^{-1}\gamma_\mu \sin\left(p_\mu\right)\right]}{12\sum_\mu \sin^2\left(p_\mu\right)}\Big|_{p^2=\mu_0^2}, \tag{8}$$

$$\left(Z_{\Gamma\Gamma'}^{\mathrm{RI/MOM}}(b,z,l,\mu_0)\right)^{-1} = \frac{\mathrm{Tr}\left[\Lambda_\Gamma(b,z,l,\mu_0)\Gamma'^\dagger\right]}{12 e^{i\mu_0\cdot(b\hat{n}_\perp + z\hat{n}_z)} Z_q^{\mathrm{RI/MOM}}(\mu_0)}, \tag{9}$$

where $S(p) = (S_u(p) + S_d(d))/2$ is the average of the up and down quark propagators and Λ_Γ is the amputated vertex function defined as

$$\Lambda_\Gamma(b,z,l,\mu_0) = \langle S_u(p)^{-1} G_\Gamma(b,z,l,\mu_0) S_d(p)^{-1}\rangle, \tag{10}$$

$$G_\Gamma(b,z,l,\mu_0) = \sum_{\mathbf{x}_f,\mathbf{x}} e^{-i\mu_0\cdot(x_f - x_0)}\langle u(x_f)\bar{u}(x)\Gamma \mathcal{W} d(x + b\hat{n}_\perp + z\hat{n}_z)\bar{d}(x_0)\rangle. \tag{11}$$

According to symmetry arguments, staple-shaped operators of different Dirac structures can and will mix; thus, the renormalization function $Z_{\Gamma\Gamma'}^{\mathrm{RI/MOM}}$ takes a matrix form. In order to define all matrix elements of $Z_{\Gamma\Gamma'}^{\mathrm{RI/MOM}}$, we make use of a number of different projectors Γ' (see Eq. 9).

The conversion to the $\overline{MS}$ reference scheme (commonly used in the analysis of experimental data) requires the perturbative computation of the matching function and is postponed to an upcoming publication [9].

3. Results

3.1 Bare matrix elements

Matrix elements are subject to excited state contamination and we check convergence by comparing their value measured at various source-sink time separations t_s. In Fig. 2, we show the pion matrix elements of the operator $\Gamma = \gamma_4$ and staple parameters $b/a = 1$, $z/a = 5$ and $l/a = 4$.

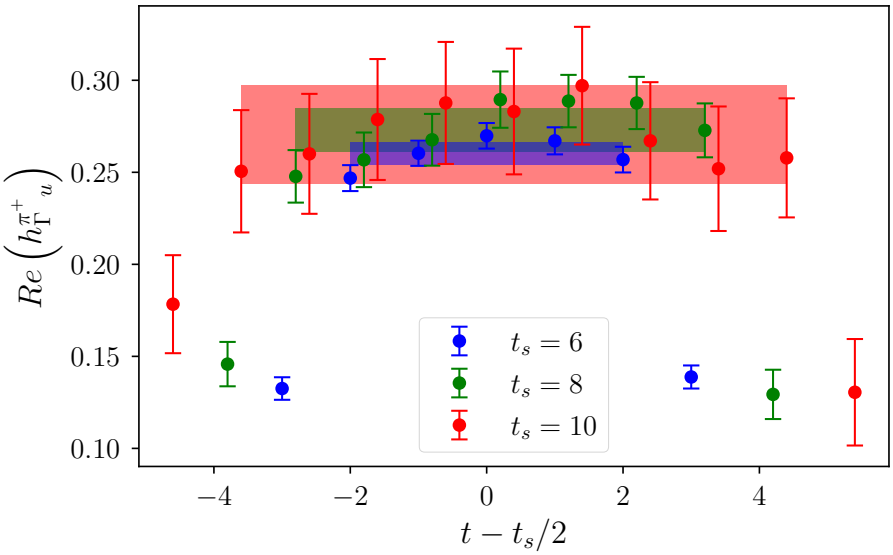

Figure 2: The real part of the bare pion matrix element of the operator $\Gamma = \gamma_4$ with staple parameters $b/a = 1$, $z/a = 5$ and $l/a = 4$ for source-sink time separations $t_s = 6a$ (blue circles), $t_s = 8a$ (green circles) and $t_s = 10a$ (red circles). The plateau fits over the corresponding ranges are also shown with the corresponding colors.

We obtain consistent results within error for source-sink time separations $t_s = 6a$ to $t_s = 10a$. Since the plateau fit range varies for every source-sink time separation t_s, for all the following results presented in this work the fitting range is chosen individually for each t_s and each set of staple parameters b,z and l.

As already mentioned in the previous sections, the staple-shaped Wilson line of the insertion operator introduces linear and logarithmic divergences into the three-point function, which are visible for non-zero values of the staple parameters b, z and l. As it can be seen, in Fig. 3, there is a strong dependence of the bare results on the parameter l, which is not physical. The multiplicative RI/MOM procedure will cancel also these divergences, since the vertex functions from which the RI/MOM renormalization functions are calculated present the same linear and logarithmic divergences (see Fig. 5 in the next section).

3.2 Renormalized matrix elements

We calculated the vertex functions of Eqs. (10), (11) with momentum sources and Landau gauge-fixed configurations. We employed a total of 10 configurations and a democratic choice for the scale $\mu_0 = \left(4, 4, 4, \left(4 + \frac{1}{2}\right) L/T\right) 2\pi/L$ with half-twist in the temporal direction.

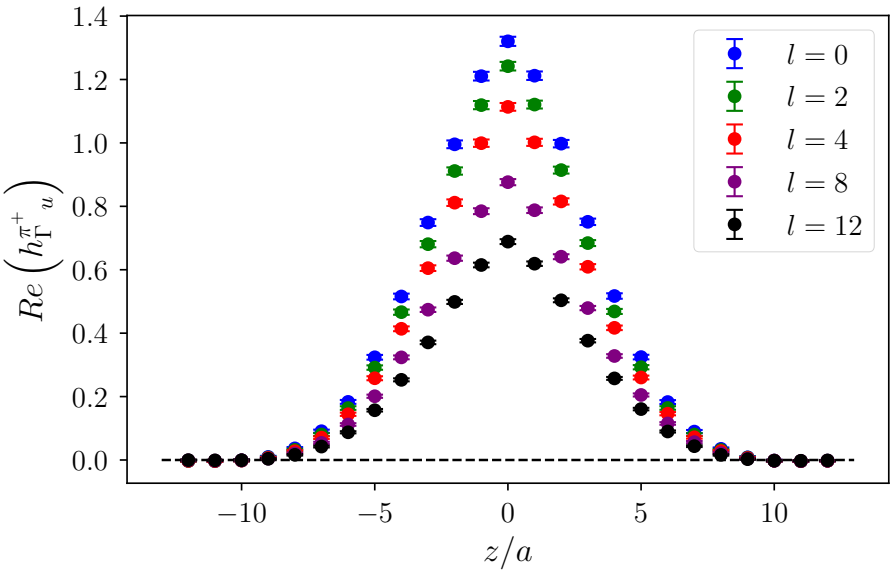

Figure 3: The real part of the bare matrix element for the operator $\Gamma = \gamma_4$ with staple parameter $b/a = 1$ and source-sink time separation $t_s = 6a$.

To identify the set of operators which mix, we have considered symmetries of the twisted mass lattice action that we employ. These include generalized parity in the α-direction ($\alpha = 1, 2, 3, 4$) combined with a discrete flavor rotation or sign change of the twisted mass term, generalized time reversal in the α-direction (again with a corresponding flavor transformation) and charge conjugation. For more details of this analysis, we refer to an upcoming publication [9]. The number of allowed mixing operators differs according to the shape of the staple. The expected mixing pattern for a staple-shaped operator whose transverse direction is $\hat{n}_x$ and the longitudinal that is parallel to the hadron boost is $\hat{n}_z$ is:

$$\begin{aligned}
&\text{Ultralocal } (b = 0,\ z = 0,\ l = 0) : \text{no mixing} \\
&\text{Straight Wilson line } (b = 0,\ l = 0) : (\mathbf{1}, \gamma_3)\,, (\gamma_5\gamma_4, \sigma_{12})\,, (\gamma_5\gamma_1, \sigma_{42})\,, (\gamma_5\gamma_2, \sigma_{41}) \\
&\text{Symmetric staple } (z = 0) : (\gamma_5\gamma_1, \gamma_5\gamma_3, \gamma_5)\,, (\gamma_1, \gamma_3, \sigma_{13})\,, (\gamma_4, \sigma_{41}, \sigma_{43})\,, (\gamma_2, \sigma_{12}, \sigma_{23}) \\
&\text{Asymmetric staple} : (\sigma_{24}, \gamma_5\gamma_1, \gamma_5\gamma_3, \gamma_5)\,, (\mathbf{1}, \gamma_1, \gamma_3, \sigma_{13})\,, \\
&\qquad (\gamma_4, \sigma_{41}, \sigma_{43}, \gamma_5\gamma_2)\,, (\gamma_2, \sigma_{12}, \sigma_{23}, \gamma_5\gamma_4)\,. \qquad (12)
\end{aligned}$$

Considering the expected mixing sets, we are able to extract the renormalization functions of the staple-shaped operators under study. The procedure consists in the inversion of a sub-matrix of the total projected vertex function matrix (see denominator of the right-hand side of Eq. (9)), whose indices, both for the operator and the projector, correspond to the matrices present in one of the expected mixing sets presented in Eq. (12). The results of $Z^{\text{RI/MOM}}_{V_0} = Z^{\text{RI/MOM}}_{\gamma_4\gamma_4}$ for the symmetric and asymmetric staples are shown in Fig. 4 for the transverse staple parameter $b/a = 1$. The linear and logarithmic divergences aforementioned in previous sections of this work, generated by the staple-shaped Wilson line in the vertex function (see Eq. (11)), affect significantly the renormalization function dependence on the staple parameters b, z and l. Fig. 4 depicts specifically the strong

dependence on the parameters z and l.

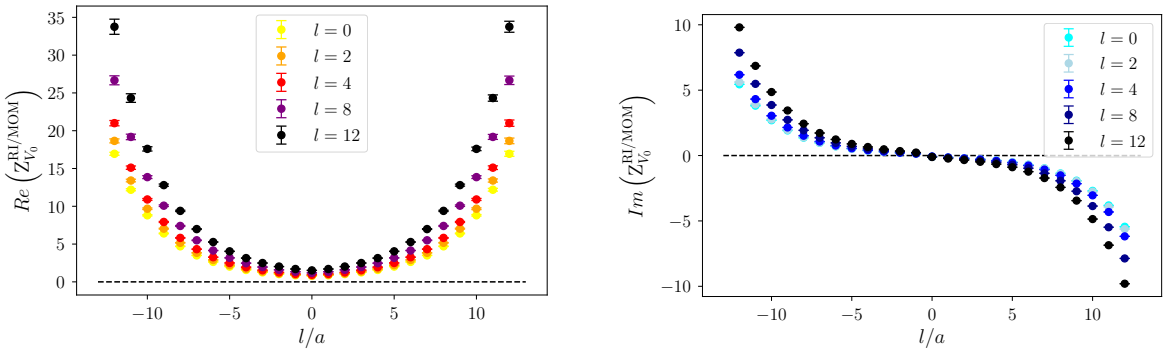

Figure 4: Real (left) and imaginary (right) parts of $Z_{V_0}^{\mathrm{RI/MOM}} = Z_{\gamma_4\gamma_4}^{\mathrm{RI/MOM}}$ for different values of l at $b/a = 1$.

By using the renormalization matrix and taking into account the mixing sets of operators, we calculate the renormalized matrix elements in the RI/MOM scheme as follows:

$$h_{\Gamma\ u}^{M\,\mathrm{RI/MOM}} = \sum_{\Gamma'} Z_{\Gamma\Gamma'}^{\mathrm{RI/MOM}} h_{\Gamma'\,u}^{M}\,. \tag{13}$$

The behavior of the renormalized matrix elements with respect to the staple parameter l is shown in Fig. 5 for π^+ for the operator $\Gamma = \gamma_4$, time separation $t_s = 6$ and transverse staple parameter $b/a = 1$. The cancellation of all linear and logarithmic divergences, introduced by the staple-shaped Wilson line, by the combination of bare matrix elements and RI/MOM renormalization functions happens as expected. In the following renormalized results, we employ a plateau fit over the asymptotic limit range of l for every set of staple parameters b, z, insertion operator Γ and source-sink time-separation t_s.

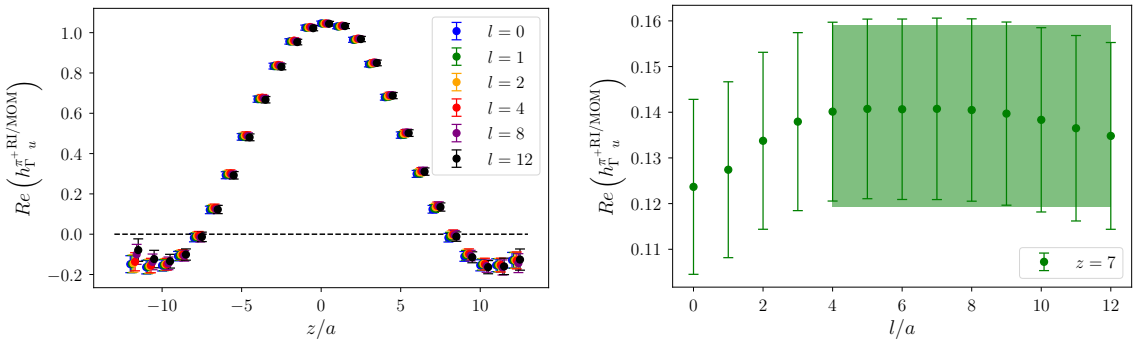

Figure 5: Left: The real part of the RI/MOM renormalized matrix element for the operator $\Gamma = \gamma_4$ with staple parameter $b/a = 1$ and source-sink time separation $t_s = 6$. The renormalized result is independent of the staple parameter l. Right: the values of the renormalized matrix element at $z/a = 7$ as a function of l/a. The band shows the weighted average starting from $l/a = 4$.

The RI/MOM renormalized matrix elements of both π^+ and K^+ for the insertion operator $\Gamma = \gamma_4$ and transverse staple parameter $b/a = 1$ are presented in Fig. 6. It is worth mentioning that these results are calculated from symmetrized bare matrix elements, since the slight asymmetry of the

bare matrix element results grows significantly once combined with the exploding dependence of the RI/MOM renormalization functions for increasing values of b,z and l.

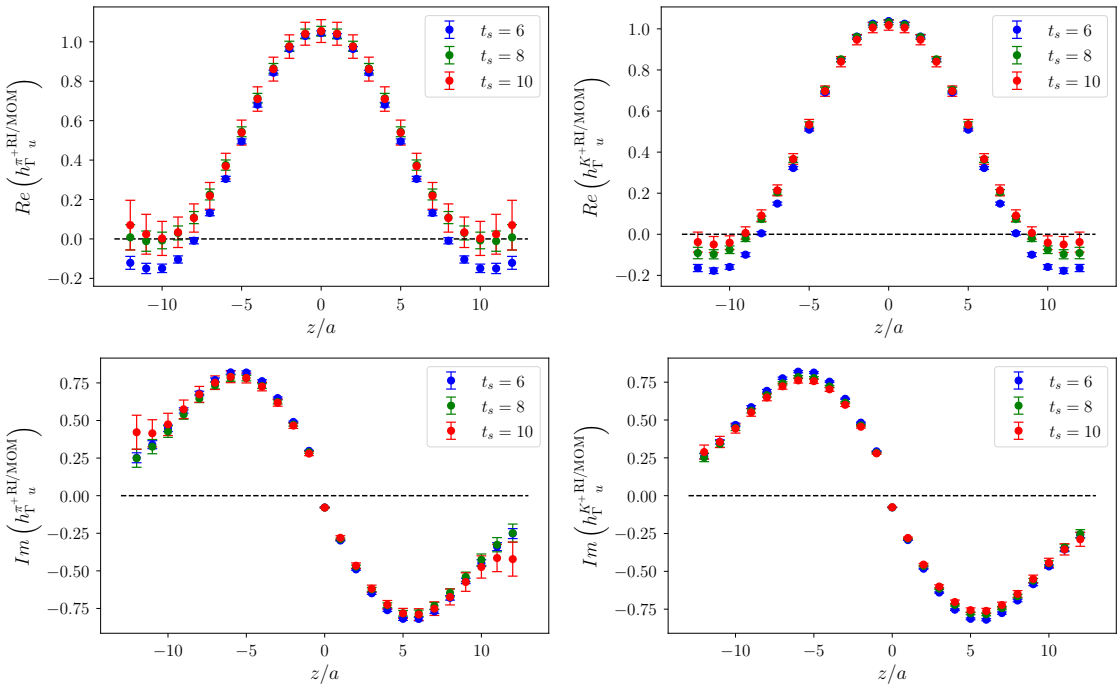

Figure 6: Real (top panels) and imaginary (bottom panels) parts of the RI/MOM renormalized matrix elements of π^+ (left panels) and K^+ (right panels). The source-sink time separations are $t_s = 6a$ (blue circles), $t_s = 8a$ (green circles) and $t_s = 10a$ (red circles).

4. Conclusions

Preliminary results for TMDPDFs of the pion and the kaon are presented. The RI/MOM renormalized results are shown to be independent of the staple parameter l for all values of the staple parameter z.

Future work includes the analysis of additional meson boosts, the perturbative subtraction of the lattice artifacts from the renormalization factors, and the conversion to the $\overline{MS}$ scheme. We then intend to combine our previous results for the soft function [17] and quasi-beam functions together with Collins-Soper kernels, in order to provide a full calculation of the TMDPDFs for the pion and kaon. Investigation of different ensembles with lighter pion masses as well as the investigation of the dependence on the finite lattice spacing are also planned.

Acknowledgments

J.T. was funded by project NextQCD, co-funded by the European Regional Development Fund and the Republic of Cyprus through the Research and Innovation Foundation (EXCELLENCE/0918/0129), and the 3D-nucleon [EXCELLENCE/0421/0043] . S.B. is supported by the H2020 project PRACE 6-IP (grant agreement No. 82376) and the EuroCC project (grant agreement No. 951740). G.S.

acknowledges financial support from the H2020 project PRACE 6-IP (GA No. 823767). A.S and F.S were funded by the NSFC and the Deutsche Forschungsgemeinschaft (DFG, German Research Foundation) through the funds provided to the Sino-German Collaborative Research Center TRR110 "Symmetries and the Emergence of Structure in QCD" (NSFC Grant No. 12070131001, DFG Project-ID 196253076 - TRR 110). K.C. is supported by the National Science Centre (Poland) grant SONATA BIS No. 2016/22/E/ST2/00013 and OPUS grant No. 2021/43/13/ST2/00497. M.C. acknowledges financial support by the U.S. Department of Energy, Office of Nuclear Physics, Early Career Award under Grant No. DE-SC0020405. X.F. is supported in part by NSFC of China under Grant No. 11775002 and National Key Research and Development Program of China under Contracts No. 2020YFA0406400. X.F. and C.L. are supported in part by NSFC of China under Grant No.12070131001. C.L. is supported in part by CAS Interdisciplinary Innovation Team and NSFC of China under Grant No. 11935017.

References

[1] M. Anselmino, M. Guidal, P. Rossi, Topical issue on the 3-D structure of the nucleon. Eur. Phys. J. A 52 (2016) 164. doi:10.1140/epja/i2016-16164-4.

[2] X. Ji, Phys. Rev. Lett. **110** (2013), 262002 doi:10.1103/PhysRevLett.110.262002 [arXiv:1305.1539 [hep-ph]].

[3] K. Cichy, M. Constantinou, Adv. High Energy Phys. 2019 (2019) 3036904, doi:10.1155/2019/3036904 [arXiv:1811.07248 [hep-lat]]

[4] X. Ji, Y.-S. Liu, Y. Liu, J.-H. Zhang, Y. Zhao. Rev. Mod. Phys., 93(3):035005, 2021. doi: 10.1103/ RevModPhys.93.035005.

[5] M. Constantinou, Eur. Phys. J. A 57 (2021) 77, doi:10.1140/epja/s10050-021-00353-7 [arXiv:2010.02445 [hep-lat]]

[6] K. Cichy, PoS LATTICE2021 (2022) 017, doi:10.22323/1.396.0017 [arXiv:2110.07440 [hep-lat]]

[7] K. Cichy, EPJ Web Conf. 258 (2022) 01005, doi:10.1051/epjconf/202225801005 [arXiv:2111.04552 [hep-lat]]

[8] X. Ji, Y. Liu and Y. S. Liu, Phys. Lett. B **811** (2020), 135946 doi:10.1016/j.physletb.2020.135946 [arXiv:1911.03840 [hep-ph]].

[9] C. Alexandrou et al., in preparation.

[10] C. Alexandrou, S. Bacchio, P. Charalambous, P. Dimopoulos, J. Finkenrath, R. Frezzotti, K. Hadjiyiannakou, K. Jansen, G. Koutsou and B. Kostrzewa, *et al.* Phys. Rev. D **98** (2018) no.5, 054518 doi:10.1103/PhysRevD.98.054518 [arXiv:1807.00495 [hep-lat]].

[11] G. S. Bali, B. Lang, B. U. Musch and A. Schäfer, Phys. Rev. D **93** (2016) no.9, 094515 doi:10.1103/PhysRevD.93.094515 [arXiv:1602.05525 [hep-lat]].

[12] C. Alexandrou, F. Jegerlehner, S. Güsken, K. Schilling, R. Sommer, Phys. Lett. B 256, 60 (1991).

[13] M. Falcioni, M. L. Paciello, G. Parisi, B. Taglienti (APE Collaboration), Nucl. Phys. B 251, 624 (1985).

[14] C. Morningstar, M. J. Peardon, QCD, Phys. Rev. D69 (2004) 054501 [hep-lat/0311018].

[15] P. Shanahan, M. L. Wagman and Y. Zhao, Phys. Rev. D **101** (2020) no.7, 074505 doi:10.1103/PhysRevD.101.074505 [arXiv:1911.00800 [hep-lat]].

[16] G. Martinelli, C. Pittori, C. Sachrajda, M. Testa, A. Vladikas. Nucl. Phys. B, 445:81–108, 1995. doi: 10.1016/0550-3213(95)00126-D.

[17] Y. Li, S. C. Xia, C. Alexandrou, K. Cichy, M. Constantinou, X. Feng, K. Hadjiyiannakou, K. Jansen, C. Liu and A. Scapellato, *et al.* Phys. Rev. Lett. **128** (2022) no.6, 062002 doi:10.1103/PhysRevLett.128.062002 [arXiv:2106.13027 [hep-lat]].